

## Electronic structure and temperature-induced paramagnetism in $\text{LaCoO}_3$

T. Saitoh,\* T. Mizokawa, and A. Fujimori

*Department of Physics, University of Tokyo, Bunkyo-ku, Tokyo 113, Japan*

M. Abbate

*Laboratorio Nacional de Luz Sincrotron, Caixa Postal 6192, Campinas, 13081-970, Brazil*

Y. Takeda

*Department of Chemistry, Faculty of Engineering, Mie University, Tsu 514, Japan*

M. Takano

*Institute for Chemical Research, Kyoto University, Uji, Kyoto 611, Japan*

(Received 10 June 1996; revised manuscript received 3 September 1996)

We have studied the electronic structure of  $\text{LaCoO}_3$  by photoemission spectroscopy and x-ray absorption spectroscopy (XAS). The Co  $2p$  core-level and valence-band photoemission spectra display satellite structures indicating a strong electron-correlation effect. The Co  $2p$  core-level photoemission, the valence-band photoemission, and the O  $1s$  XAS spectra have been analyzed using a configuration-interaction cluster model for the initial-state configurations of the low-spin (LS:  $^1A_1$ ), intermediate-spin (IS:  $^3T_1$ ) and high-spin (HS:  $^5T_2$ ) states and their mixtures. The ground state of  $\text{LaCoO}_3$  in the LS state is found to have heavily mixed  $d^6$  and  $d^7L$  character, reflecting the strong covalency. The magnetic susceptibility has been analyzed for various level orderings of the LS, IS, and HS states. From the analyses of the photoemission spectra and the magnetic susceptibility data, the temperature-induced paramagnetism in  $\text{LaCoO}_3$  above  $\sim 90$  K is most likely due to a gradual LS-to-IS transition. [S0163-1829(97)01607-X]

### I. INTRODUCTION

$3d$  transition-metal (TM) perovskite oxides have been the subject of many structural, magnetic, and transport studies since 1950's. Recent interest in strongly correlated systems has brought about further extensive research in these compounds including  $\text{LaCoO}_3$  studied here.  $\text{LaCoO}_3$  is unique in that it is a nonmagnetic semiconductor at low temperatures but undergoes a gradual transition to a paramagnetic state above  $\sim 90$  K and to a metal above  $\sim 500$  K. Although there have already been many studies on these phenomena, their underlying electronic structure and spin states have not been clarified. Especially, it remains highly controversial whether the 90-K transition is a low-spin-to-high-spin transition or not.<sup>1,2</sup> The purpose of the present work is to investigate the origin of the gradual nonmagnetic-to-paramagnetic transition using electron spectroscopic methods.

The magnetic susceptibility  $\chi$  of  $\text{LaCoO}_3$  increases with temperature and shows a maximum at  $\sim 90$  K, above which it becomes Curie-Weiss-like. There is also a plateau around 500 K, above which the Curie constant increases.<sup>3-5</sup> Neutron diffraction studies have revealed that no long-range magnetic order exists down to 4.2 K,<sup>6</sup> indicating that the ground state of  $\text{LaCoO}_3$  is nonmagnetic, namely, the  $\text{Co}^{3+}$  ion is in the low-spin ( $t_{2g}^6 e_g^0$ :  $^1A_1$ ) configuration. Naiman *et al.* and Jonker<sup>7</sup> have proposed the formation of the high-spin ( $^5T_2$  or  $t_{2g}^4 e_g^2$ ) configuration by thermal activation and explained their  $\chi$ - $T$  data. Raccach and Goodenough<sup>3</sup> have considered that the low-spin-to-high-spin transition occurs at a plateau around 500 K from their x-ray diffraction data, which indi-

cated that the crystal structure has  $R\bar{3}c$  symmetry below 648 K and  $R\bar{3}$  above 648 K. However, a neutron diffraction study in the range  $4.2 < T < 1248$  K by Thornton, Tofield, and Hewat<sup>8</sup> has shown that the symmetry is  $R\bar{3}c$  at all measured temperatures except for at 668 K where they concluded that the symmetry may be  $R\bar{3}$ . Recent neutron diffraction and NMR studies have revealed that a nonmagnetic-to-paramagnetic transition occurs at about 90 K.<sup>1,9</sup> The electrical conductivity  $\sigma$  is of the thermal activation type with an activation energy of  $\sim 0.1$  eV at low temperatures and gradually changes to a metallic one through a plateau between 620 and 750 K.<sup>10-12</sup> Local-density-approximation (LDA) band-structure calculation<sup>13</sup> has predicted a valence-band density of states (DOS) that is in good agreement with the x-ray photoemission spectroscopy (XPS) spectra except that they give a semimetallic state and show no satellite structures.<sup>14</sup> Band-structure calculations using the LDA+ $U$  method<sup>15</sup> and unrestricted Hartree-Fock calculations on the multiband Hubbard model<sup>16</sup> have shown that the intermediate-spin and the high-spin states exist only slightly above the nonmagnetic ground state.

So far many photoelectron spectroscopic studies have been reported on  $\text{LaCoO}_3$ .<sup>2,17-23</sup> Lam, Veal and Ellis<sup>18</sup> have measured the XPS spectra of  $\text{LaCoO}_3$  at room temperature and 573 K and suggested from ionic multiplet analysis that the low-spin and the high-spin states coexist at room temperature. Richter, Bader, and Brodsky have also observed a temperature-dependent change in the ultraviolet photoemission spectroscopy (UPS) spectra.<sup>19</sup> Recently, Chainani, Mathew and Sarma<sup>21</sup> investigated the XPS, UPS, and brems-

strahlung isochromat spectroscopy (BIS) spectra of  $\text{La}_{1-x}\text{Sr}_x\text{CoO}_3$ , and obtained the charge-transfer energy  $\Delta$ , the  $3d$ - $3d$  Coulomb interaction  $U$ , and the O  $2p$ -Co  $3d$  hybridization ( $pd\sigma$ ) of 4.0, 3.4, and 2.2 eV, respectively, for  $\text{LaCoO}_3$  by analyzing the Co  $2p$  core-level spectrum with configuration-interaction (CI) cluster-model calculations. They have estimated the band gap of  $\text{LaCoO}_3$  to be about 0.6 eV from the UPS and BIS spectra.<sup>21</sup> Abbate *et al.*<sup>2</sup> have reported that the O  $1s$  x-ray absorption (XAS) spectra show no difference between  $\sim 80$  and 300 K while a new structure appears above  $\sim 500$  K, and have interpreted this latter change as a temperature-induced low-spin-to-high-spin transition. Their report has aroused controversy because the neutron and NMR studies claim that the low-spin-to-high-spin transition occurs around  $\sim 90$  K.<sup>1,9</sup> Barman and Sarma<sup>23</sup> have measured high- and low-temperature XPS and UPS spectra and concluded that their data are consistent with the neutron measurement. Hence, how the effect of magnetic transition appears in photoemission spectra is still unclear and it is worthwhile to further investigate  $\text{LaCoO}_3$ .

In this paper, we present the results of our XPS, UPS, resonant photoemission, and XAS studies as well as an analysis of the  $\chi$ - $T$  data. In order to elucidate the magnetic behavior of  $\text{LaCoO}_3$ , we put emphasis on the analysis of  $\chi$ - $T$  data and CI cluster-model calculations, both of which take into account not only the low-spin ( $t_{2g}^6 e_g^0$ :  $^1A_1$ ) and high-spin ( $t_{2g}^4 e_g^2$ :  $^5T_2$ ) states but also the intermediate-spin ( $t_{2g}^5 e_g^1$ :  $^3T_1$ ) state.

## II. EXPERIMENT

Polycrystalline samples of  $\text{LaCoO}_3$  were prepared by solid-state reaction. Sintered mixtures of appropriate molar quantities of well-dried  $\text{La}_2\text{O}_3$  and  $\text{Co}_3\text{O}_4$  were pressed into pellets. Subsequently, the pellets were fired in  $\text{O}_2$  atmosphere at 900 °C for 48 h, at 1200 °C for 24 h, and at 1300 °C for 24 h, and then slowly cooled to room temperature. The magnetic susceptibility was measured using a Quantum Design superconducting-quantum-interference-device (SQUID) magnetometer.

XPS and UPS (He I:  $h\nu=21.2$  eV) measurements were carried out using a spectrometer equipped with a Mg  $K\alpha$  source, a He discharge lamp, and a Physical Electronics (PHI) double-pass cylindrical mirror analyzer. All the XPS spectra have been corrected for the Mg  $K\alpha_{3,4}$  ghost. UPS spectra were measured using a Vacuum Science Workshop (VSW) hemispherical analyzer and the He II line ( $h\nu=40.8$  eV). UPS spectra including  $3p$ - $3d$  resonant-photoemission spectra were also measured at beamline BL-2 of Synchrotron Radiation Laboratory (SRL), Institute for Solid State Physics, University of Tokyo. XAS spectra were taken at beam-line BL-2B of Photon Factory (PF), National Laboratory for High Energy Physics. All the measurements using the PHI system and those at SRL were carried out at liquid-nitrogen temperatures ( $\sim 80$  K). The measurements using the VSW system and those at PF were done at various temperatures ranging from  $\sim 30$  K to room temperature. Binding energies of the photoemission spectra have been calibrated using the Fermi edge of Au evaporated onto samples. Photon energies for the XAS spectra have been calibrated using the O  $1s$  absorption peak of  $\text{TiO}_2$  at 530.7

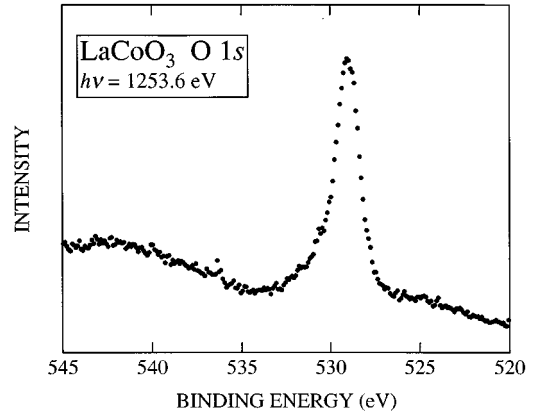


FIG. 1. O  $1s$  core-level XPS spectrum of  $\text{LaCoO}_3$ . The broad peak around 540 eV is due to Co  $L_3M_{23}V$  and La  $M_{45}N_{45}V$  Auger emissions.

eV. The energy resolutions of the XPS and He I UPS were  $\sim 0.9$  and  $\sim 0.25$  eV full width at half maximum (FWHM), respectively. In the case of the UPS measurements using the VSW system, it was  $\sim 80$  meV for He II. The energy resolution of the measurements at SRL was 0.3–0.4 eV FWHM for photon energies from 40 to 80 eV. In the XAS measurements, the resolution was  $\sim 0.2$  eV.

For surface cleaning, we have scraped the surfaces of the samples with a diamond file *in situ* at measurement temperatures. The O  $1s$  core-level spectrum of  $\text{LaCoO}_3$  (Fig. 1) shows no shoulder on the higher binding energy side,<sup>19</sup> indicating that a clean surface was obtained. In the case of UPS, the scraping was repeated until a bump around 9–10 eV disappeared and the whole spectrum did not change with further scraping.

## III. RESULTS

### A. Magnetic susceptibility

Figure 2(a) shows the experimental  $\chi$ - $T$  curve and curves calculated using three models, namely, the  $^1A_1$ - $^5T_2$  two-state (LH) model, the  $^1A_1$ - $^3T_1$  two-state (LI) model, and the  $^1A_1$ - $^3T_1$ - $^5T_2$  three-state (LIH) model, where L, I, and H denote the low-spin ( $^1A_1$ ), intermediate-spin ( $^3T_1$ ), and high-spin ( $^5T_2$ ) states, respectively. The result is in good agreement with the previous reports.<sup>9,10,12</sup> Although theoretical studies on the spin-state transitions beyond the simple ionic model, which took into account magnetic interaction between neighbor sites or the spin-orbit interaction, are available,<sup>24</sup> we have analyzed our data within the simple ionic model in order to know how well they explain the experimental result.

The  $\chi$ - $T$  curve of the two-state models (LI and LH) can be written as

$$\chi = \frac{N_A \mu_B^2 g^2 S(S+1)(2S+1)d}{3\mathcal{M}[e^{\beta E_a} + (2S+1)d]} \beta, \quad (1)$$

in units of emu/g, where  $\beta=1/kT$ , and  $N_A$  and  $\mathcal{M}$  are Avogadro number and the molar weight of  $\text{LaCoO}_3$ , respectively.  $S$  and  $d$  are the total spin and the orbital degeneracy of the  $^3T_1$  or  $^5T_2$  states.  $g$  is the  $g$  factor, which we fix to 2.0.  $E_a$  is the activation energy from the  $^1A_1$  to the  $^3T_1$  or

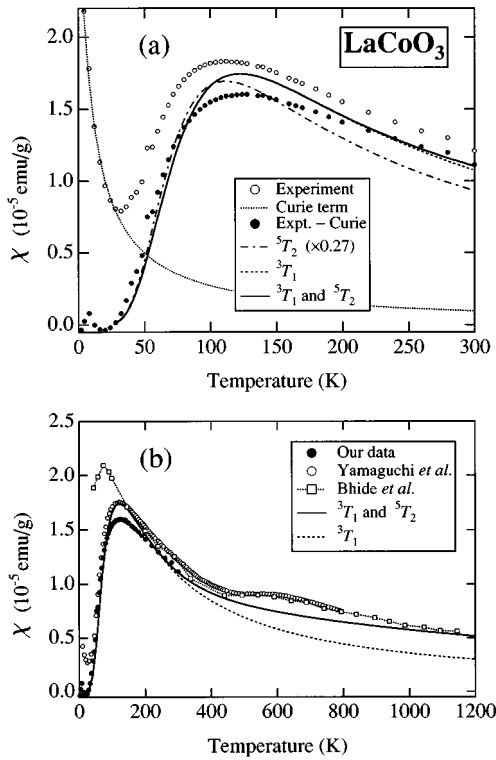


FIG. 2. (a) Magnetic susceptibility of  $\text{LaCoO}_3$ . Applied magnetic field was 10 kOe. Dot-dashed line ( ${}^5T_2$ ): the  ${}^1A_1$ - ${}^5T_2$  two-state (LH) model with an activation energy  $E_a$  of 266 K. Note that the magnitude is reduced by a factor of 0.27. Dashed line ( ${}^3T_1$ ): the  ${}^1A_1$ - ${}^3T_1$  two-state (LI) model with an activation energy  $E_a$  of 257 K. Solid line ( ${}^3T_1$  and  ${}^5T_2$ ): the  ${}^1A_1$ - ${}^3T_1$ - ${}^5T_2$  three-state (LIH) model with an activation energies 257 K ( $E_{a1}$ ) and 1731 K ( $E_{a2}$ ). (b) LI model (dashed line) and LIH model (solid line) compared with the previous experimental data (filled circles), Yamaguchi *et al.* (Ref. 12) (open circles) and Bhide *et al.* (Ref. 10) (open squares).

${}^5T_2$  state. The LIH model can be described in a way similar to Eq. (1). The Curie-Weiss term due to impurities<sup>9</sup> (with a Curie constant of  $2.9 \times 10^{-4}$  emu K/g and a Weiss temperature of  $-9.3$  K) was subtracted from the raw data as shown in Fig. 2(a). One can see from Fig. 2(a) that an activation energy  $E_a$  of about 260 K is needed in any model in order to produce the peak at  $\sim 90$  K and that the LH model cannot reproduce its peak height. By contrast, the LI and the LIH models can simulate both the position and the peak height. In fact, Heikes, Miller, and Nazelsky have explained their  $\chi$ - $T$  curve from  $\sim 100$  to  $\sim 1000$  K by a model in which electrons are thermally excited from a  $S=1$  ground state to  $S=2$  or  $S=3/2$  states.<sup>5</sup> Their analysis suggests that at high temperatures (above  $\sim 500$  K), a model including the high-spin state may describe the experiment. In Fig. 2(b), the LI and LIH models are compared with the experimental data of Bhide *et al.*<sup>10</sup> and Yamaguchi *et al.*<sup>12</sup> up to  $\sim 1000$  K. Above  $\sim 800$  K, the LIH model shows better agreement with experiment than the LI model, although both models fail to reproduce the plateau around 500 K. Here it should be noted that we have assumed the  $E_a$  to be temperature independent for simplicity although thermal expansion reduces the crystal-field splitting and lowers the  $E_a$  as assumed by Korotin *et al.*<sup>15</sup> Furthermore, a transition to the intermediate-spin (IS)

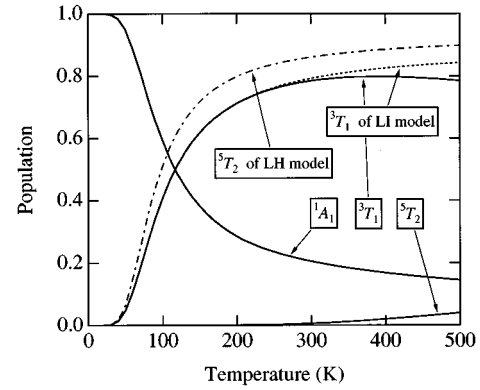


FIG. 3. Population of the  ${}^5T_2$  level in the LH model (dot-dashed line), the  ${}^3T_1$  level in the LI model (dashed line) and the  ${}^1A_1$ ,  ${}^3T_1$ , and  ${}^5T_2$  levels in the LIH model (solid line).  $E_a$ 's are the same as those in Fig. 2.

or high-spin (HS) state will change the radius of the  $\text{Co}^{3+}$  ion, leading to a change in  $E_a$ .<sup>1</sup> This would have a particularly pronounced effect on the transition to the HS state around  $\sim 500$  K (Ref. 2) and would cause a more drastic change in the population of the HS state as a function of temperature than predicted here. Nevertheless, the thermal expansion should be less important for the  $\sim 90$ -K transition because of the low temperature and the temperature-independent  $E_a$  would be a good approximation for the present analysis.

Recently, Itoh *et al.* have investigated a model based on the LH model taking into account level splittings due to the trigonal distortion of the crystal structure and the spin-orbit interaction.<sup>25</sup> However, these effects could not reduce the magnitude of the peak height and they inferred the presence of antiferromagnetic coupling between the local (high) spins.<sup>25</sup> Our analysis suggests that the LI or the LIH models give fair agreement with experiment in spite of their simplicity, encouraging us to proceed further without the spin-orbit interaction and the trigonal distortion. The LDA+ $U$  (Ref. 15) and Hartree-Fock (Ref. 16) calculations also suggest that the intermediate-spin state can be the first excited magnetic level. It should be emphasized, however, that these ionic models are too simplistic because the Co  $3d$  orbitals in fact strongly hybridize with the O  $2p$  orbitals due to the small charge-transfer energy,<sup>26</sup> as described below.

We show the thermal population of the excited levels in the three models in Fig. 3. In any model, the population of the  ${}^1A_1$  ground state is greater than 0.9 below  $\sim 50$  K and decreases with temperature. In the LIH model, for example, this number decreases to  $\sim 0.2$  at 300 K. Hence, if each state is thermally populated and the different states ( ${}^1A_1$ ,  ${}^3T_1$ , and  ${}^5T_2$ ) produce different photoemission spectra, the spectra are expected to change with temperature. In the following sections, we will analyze the XPS, UPS, and O  $1s$  XAS spectra of  $\text{LaCoO}_3$  with CI cluster-model calculations for the  ${}^1A_1$ ,  ${}^3T_1$ , and  ${}^5T_2$  initial-state configurations. Comparison with the band-structure calculation<sup>13</sup> shall also be presented.

### B. Configuration-interaction cluster-model analysis of spectroscopic data

In order to determine the electronic structure of  $\text{LaCoO}_3$ , we have performed CI cluster-model calculations

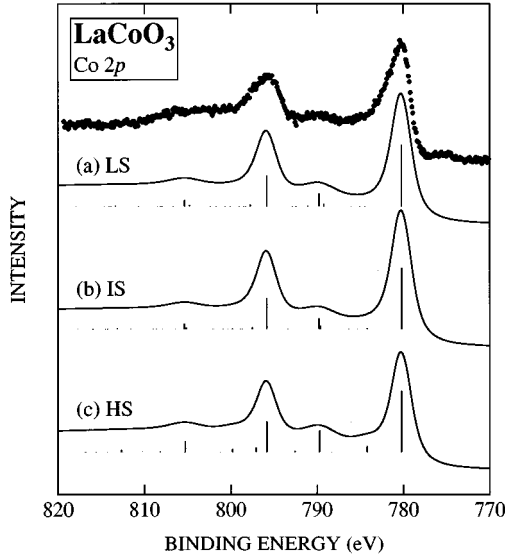


FIG. 4. Cluster-model analysis of the Co  $2p$  core-level XPS spectrum of  $\text{LaCoO}_3$  within the single Slater-determinant scheme assuming (a) the low-spin ( $t_{2g}^6 e_g^0$ : LS), (b) the intermediate-spin ( $t_{2g}^5 e_g^1$ : IS), and (c) the high-spin ( $t_{2g}^4 e_g^2$ : HS) initial states.

for the Co  $2p$  core-level photoemission, valence-band photoemission, and O  $1s$  XAS spectra. Following the analysis of the magnetic susceptibility, we have calculated spectra not only for the low-spin and the high-spin initial states, but also for the intermediate-spin initial state. The model is described by three parameters, namely, the multiplet-averaged  $d$ - $d$  Coulomb interaction  $U$ , the ligand  $p$ -to-transition-metal (TM)  $d$  charge-transfer energy  $\Delta$ , and the ligand  $p$ -TM  $d$  transfer integral ( $pd\sigma$ ).

We have performed the calculations in two ways: in one scheme we have neglected the off-diagonal matrix elements of the electron-electron interaction and retain only the diagonal part of the  $d$ - $d$  Coulomb and exchange interaction, using single Slater determinants as the wave functions. We refer to this approximation as the single Slater-determinant (SSD) scheme.<sup>26–28</sup> The other is the full-multiplet calculations, which include all the matrix elements of the electron-electron interaction, and we refer to it as the full-multiplet configuration-interaction (FMCI) scheme.<sup>29</sup> In the SSD scheme, the bases are not necessarily eigenstates of the total spin nor do they have proper point-group symmetry, but one can reduce the number of bases and hence calculate spectra for light TM compounds, which have fewer  $d$  electrons and require a much larger number of basis functions. For  $\text{LaCoO}_3$ , the SSD scheme happens to be a good approximation for the low-spin (LS) state in reproducing the experimental spectra, because the  $d^6$  LS configuration has the correct symmetry of the singlet ground state (see below). However, as will be discussed below, the energy gain of the LS state in the SSD scheme is not enough to become the ground state for reasonable parameter values because of the neglect of the  $d$ - $d$  configuration interactions, which is generally important for states where the spins are not fully polarized. In the calculations of the TM  $2p$  core-level spectra, the SSD scheme gives similar results to the FMCI scheme because of the large lifetime width of the  $2p$  peaks. Hence,

TABLE I. Parameters obtained from the CI cluster-model analysis of the Co  $2p$  core-level photoemission spectrum of  $\text{LaCoO}_3$  for the low-spin (LS), intermediate-spin (IS), and high-spin (HS) initial states within the SSD scheme (in units of eV). Racah parameters used in the analysis are  $B=0.132$  eV and  $C=0.635$  eV.

	$\Delta$	$U$	$(pd\sigma)$
LS	$2.0 \pm 2.0$	$5.5 \pm 1.0$	$-1.7 \pm 0.2$
IS	$2.0 \pm 2.0$	$5.5 \pm 1.0$	$-1.8 \pm 0.2$
HS	$1.0 \pm 2.0$	$6.8 \pm 1.0$	$-2.0 \pm 0.2$

for the Co  $2p$  core level, we have employed the SSD scheme to obtain values for the parameters  $\Delta$ ,  $U$ , and  $(pd\sigma)$ . For the valence-band photoemission and O  $1s$  XAS spectra, which require more accurate treatment of multiplet structures, we have performed calculations within the FMCI scheme.

### 1. Co $2p$ core-level photoemission spectra

Calculated Co  $2p$  photoemission spectra of  $\text{LaCoO}_3$  assuming the LS, IS, and HS initial states are compared with experiment in Fig. 4. The calculated spectra have been broadened with a binding-energy-dependent Lorentzian function and a Gaussian function.<sup>27,28,30</sup> Obtained parameters are listed in Table I. In every calculation, the main peak largely consists of  $\underline{c}d^7\bar{L}$  and  $\underline{c}d^8\bar{L}^2$  final states, where  $\underline{c}$  denotes a Co  $2p$  core hole. Although  $\Delta$  and  $(pd\sigma)$  for the high-spin state are smaller and larger than those for the LS state (Table I), respectively,  $d^7\bar{L}$  has large weight in the LS initial state compared to the HS state (Table II). This is because the LS initial state has more empty  $e_g$  orbitals, whose hybridization strength is larger than that of the  $t_{2g}$  states by a factor  $\sim 2$ .<sup>31</sup> The net  $d$ -electron number ( $N_d$ ) and the  $d$  character of doped carriers ( $C_{\text{hole}}^d$  and  $C_{\text{electron}}^d$ , where, e.g.,  $C_{\text{hole}}^d = 1$  means that the doped hole has pure  $d$  character and  $C_{\text{hole}}^d = 0$  means that it has pure  $p$  character), calculated using those parameters are listed in Table III. In every spin state,  $\Delta$  is smaller than  $U$  indicating that  $\text{LaCoO}_3$  is in the charge-transfer regime. However, one can see from the values of  $C_{\text{hole}}^d$  and  $C_{\text{electron}}^d$  that the band gaps of the LS state as well as the IS states have considerable  $p$ - $p$  character, reflecting the small  $\Delta$  value.<sup>32</sup> The  $N_d$  of each state decreases from LS to HS reflecting the decrease in the  $d^7\bar{L}$  and  $d^8\bar{L}^2$  weight in the ground state.<sup>33</sup>

### 2. Band gap and total energy

The band gap ( $E_{\text{gap}}$ ) calculated using the cluster model is listed in Table III for the LS, IS, and HS states. The calculated  $E_{\text{gap}}$  corresponds to the peak-to-peak separation in the

TABLE II. Weight of various configurations for the low-spin (LS), intermediate-spin (IS), and high-spin (HS) ground states within the SSD scheme.

	$d^6$	$d^7\bar{L}$	$d^8\bar{L}^2$
LS	29 %	53 %	17 %
IS	35 %	53 %	12 %
HS	49 %	44 %	7 %

TABLE III. Net  $d$ -electron numbers ( $N_d$ ),  $d$  characters of doped carriers ( $C_{\text{hole}}^d$  and  $C_{\text{electron}}^d$ ) and band gaps ( $E_{\text{gap}}$  in eV) calculated within the SSD scheme. Band gaps calculated using the FMCI scheme are given in the parentheses.

	$N_d$	$C_{\text{hole}}^d$	$C_{\text{electron}}^d$	$E_{\text{gap}}$
LS	6.9	0.36	0.42	0.7 (5.4)
IS	6.8	0.44	0.42	-0.4 (3.8)
HS	6.6	0.30	0.64	2.5 (4.0)

combined photoemission and BIS spectra aligned at the Fermi level ( $E_F$ ), and is estimated to be  $\sim 2-3$  eV for LaCoO<sub>3</sub> from figures in Ref. 21. The magnitude of the band gap cannot be correctly calculated within the SSD scheme because of the too small energy gain compared to the FMCI scheme, particularly for the LS state. Indeed, the magnitude of the gap of the LS state in the SSD scheme, 0.7 eV, is much smaller than the above value.

In the calculations within the FMCI scheme, we have taken into account the  $10Dq$  due to the nonorthogonality between the oxygen  $p$  and TM  $d$  orbitals and the scaling factor of 0.8 for the configuration dependence of the transfer integrals.<sup>34</sup> We have thus obtained the ground state to have  $^1A_1$  symmetry for  $\Delta=2.0$  eV,  $U=5.5$  eV, and  $(pd\sigma)=-1.8$  eV. The weight of the various configurations in the  $^1A_1$ ,  $^3T_1$ , and  $^5T_2$  states agrees with those obtained by the SSD scheme to within a few percent. The  $E_{\text{gap}}$  in the FMCI scheme, especially that for the  $^1A_1$  ground state, is much larger than those of the SSD scheme as shown in Table II, due to the greater stabilization of the  $d^6$  states. The calculated  $E_{\text{gap}}\sim 5.4$  eV is now too large compared to the experiment ( $2-3$  eV). This would probably be a shortcoming of the cluster model, particularly for the  $^1A_1$  ground state: intercluster hybridization would reduce the intracluster correlation of the  $^1A_1$  state and raise its energy, thus reducing  $E_{\text{gap}}$ .

### 3. Valence-band spectra

Figure 5 shows photoemission spectra of LaCoO<sub>3</sub> in the valence-band region for various incident photon energies. Considering that the Co  $3d$ -to-O  $2p$  relative photoionization cross sections increase with incident photon energy,<sup>35</sup> structure A has a large Co  $3d$  contribution and also structure C and shoulder D have some Co  $3d$  contribution whereas the O  $2p$  contribution is dominant in structure B. This qualitative analysis is consistent with the cluster-model calculation for the low-spin state as well as with the band-structure calculation,<sup>13</sup> as described below. From  $\sim 9$  to  $\sim 14$  eV, intensities due to satellite structures can be observed in the 80.0-eV spectrum. As for the XPS ( $h\nu=1253.6$  eV) spectrum, one cannot easily identify this feature due to the overlapping tail of the intense La  $5p$  peak, but a residual intensity appears after subtraction of the integral background.

In the following calculations, the relative energy positions of the spectra for the  $^1A_1$ ,  $^3T_1$ , and  $^5T_2$  initial states have been fixed so that the three initial states have the same total energies, although the  $^3T_1$  state is located at a somewhat higher energy compared to the  $^1A_1$  and  $^5T_2$  states. (The magnetic susceptibility implies that the three states are lo-

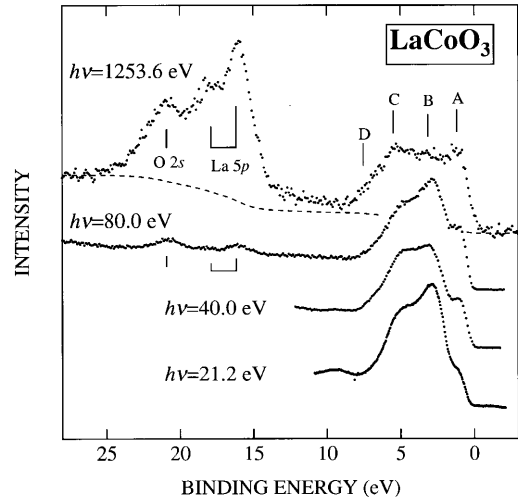


FIG. 5. Photoemission spectra of LaCoO<sub>3</sub> in the valence-band region with various incident photon energies. All the spectra were normalized to the area from  $-0.5$  to  $8.0$  eV. The integral background for the XPS spectrum (dashed line) has been obtained from  $-1.5$  to  $27.0$  eV.

cated within  $\sim 0.1$  eV.) The Co  $3d$  photoemission spectra of LaCoO<sub>3</sub> calculated using the cluster model in the FMCI scheme for the  $^1A_1$ ,  $^3T_1$ , and  $^5T_2$  initial states are shown in Fig. 6.<sup>36</sup> The  $^5T_2$  spectrum, which is spread over a wide energy range, is completely different from the  $^1A_1$  spectrum, while the  $^3T_1$  spectrum is more similar to the  $^1A_1$  spectrum. Consequently, it is expected that if the valence-band spectrum can be described as a superposition of the  $^1A_1$  and  $^3T_1$  initial states, the spectra would show only small changes with temperature.

We have also measured resonant photoemission spectra near the Co  $3p$ - $3d$  core-absorption threshold. The on- and off-resonance photon energies have been determined from the total yield (TY) spectra and constant-initial-state (CIS) spectra. In the lower panel of Fig. 6, we show on- ( $h\nu=63.5$  eV) and off- ( $h\nu=60.0$  eV) resonance spectra. The on-resonance spectrum is enhanced over a wide energy range, with the strongest enhancement from  $\sim 8$  to  $\sim 15$  eV, which can be identified as a satellite structure due to charge transfer. The on-off difference spectrum shows an intense peak near  $E_F$  and a shoulder at  $\sim 6$  eV as well as the satellite. Hence, apart from the enhancement of the satellite, the spectrum is similar to the calculated  $^1A_1$  [Fig. 6(a)] spectrum or the  $^1A_1+^3T_1$  spectrum (Fig. 7; see below). Indeed, the two structures marked with arrows in the LaCoO<sub>3</sub> spectrum correspond to the first two peaks in the  $^1A_1$  spectrum in Fig. 6(a).

In Fig. 7 are shown the valence-band XPS spectra of LaCoO<sub>3</sub> for a 70% (Ref. 1)  $A_1+30\%$   $^3T_1$  mixed initial state, corresponding to the thermal population at  $\sim 80$  K deduced from the magnetic susceptibility. In order to simulate the O  $2p$  band, we have used the He I spectrum<sup>37</sup> [Fig. 7(a)] or the calculated O  $2p$  partial DOS<sup>38</sup> [Fig. 7(b)]. The Co  $3d$ -to-O  $2p$  intensity ratios of the spectra in Figs. 7(a) and 7(b) are  $\sim 88\%$  and  $\sim 60\%$ , respectively, which are roughly equal to the calculated photoionization cross section ( $\sim 85\%$ ).<sup>35,39</sup> Both Figs. 7(a) and 7(b) show good agreement

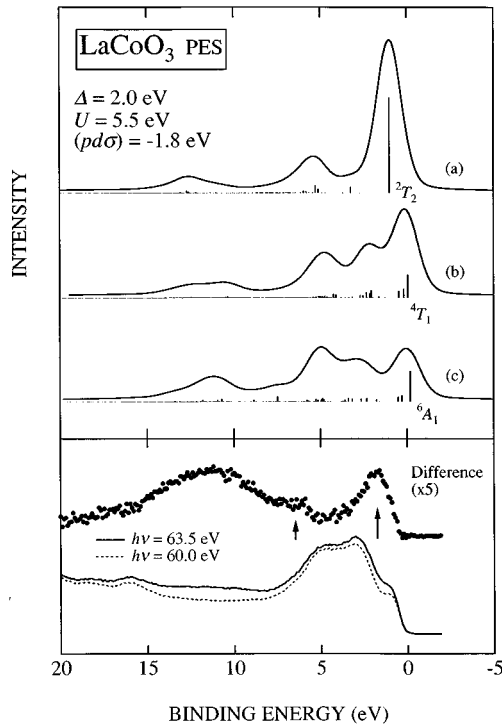


FIG. 6. Upper panel: Calculated Co 3d photoemission spectra of  $\text{LaCoO}_3$  assuming the (a)  ${}^1A_1$ , (b)  ${}^3T_1$ , and (c)  ${}^5T_2$  initial states within the full-multiplet configuration-interaction cluster model.  $\Delta = 2.0$  eV,  $U = 5.5$  eV, and  $(pd\sigma) = -1.8$  eV have been used. The position of the spectra has been determined so that the  ${}^2T_2$  final peaks are located at 1.0 eV, for simplicity. The symmetry of the first ionization states of the spectra is also shown. Lower panel: Co 3p-3d resonant photoemission spectra and the on-off difference spectrum.

between theory and experiment, with somewhat better agreement in the latter.

We also obtain good agreement between theory and experiment by assuming a 70% (Ref. 1)  $A_1 + 30\%$   ${}^5T_2$  initial state. However, the  ${}^1A_1 - {}^5T_2$  mixed spectrum is expected to strongly change with temperature, while the experimental XPS spectra have not shown appreciable changes up to  $T \sim 570$  K.<sup>2</sup> Figure 8 shows simulations of the temperature-dependent XPS spectra of  $\text{LaCoO}_3$  for the two types ( ${}^1A_1 - {}^3T_1$  and  ${}^1A_1 - {}^5T_2$ ) of mixed initial states. The ratios in the initial states have been taken from the magnetic susceptibility. One can easily see that the  ${}^1A_1 - {}^5T_2$  mixed spectrum considerably changes from  $\sim 80$  to  $\sim 300$  K, while the  ${}^1A_1 - {}^3T_1$  mixed spectrum does not change so much. Hence, we may exclude the possibility of the  ${}^1A_1 - {}^5T_2$  mixed initial state in  $\text{LaCoO}_3$ .

#### 4. O 1s XAS spectra

Figure 9 shows O 1s XAS spectra at low ( $\sim 55$  K) and high ( $\sim 300$  K) temperatures. The overall spectral features (not shown) are in good agreement with the previous report,<sup>2</sup> with the peak at 529.4 eV attributed to the empty Co 3d band hybridizing with the O 2p band. One can find from Fig. 9 that the intensity around the peak slightly decreases with temperature while an increase in the weight is seen around

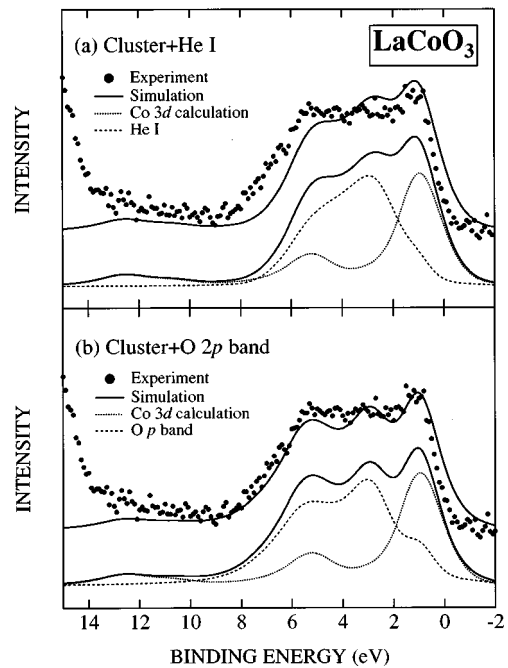


FIG. 7. Full-multiplet cluster-model analyses of the valence-band XPS spectra of  $\text{LaCoO}_3$  assuming the 70%  ${}^1A_1 + 30\%$   ${}^3T_1$  initial states. The calculated valence-band spectra (solid lines) are compared with the experimental spectra (dots). Dotted lines are the calculated Co 3d spectra and the dashed lines are simulation of the O 2p partial DOS taken from the He I spectrum of  $\text{LaCoO}_3$  (a) or the calculated O 2p partial DOS by Hamada, Sawada, and Terakura (Ref. 13) (b).

528.4 eV, where Abbate *et al.* observed a prominent growth of a structure above 550 K.<sup>2</sup> We cannot conclude, however, whether the shoulder at 300 K in our data and the low-energy structure observed by Abbate *et al.* have the same origin or not. A very recent optical study has revealed that the temperature-dependent optical spectra of  $\text{LaCoO}_3$  show dramatic changes above room temperature in a wide energy range of several electron volts in spite of very small changes

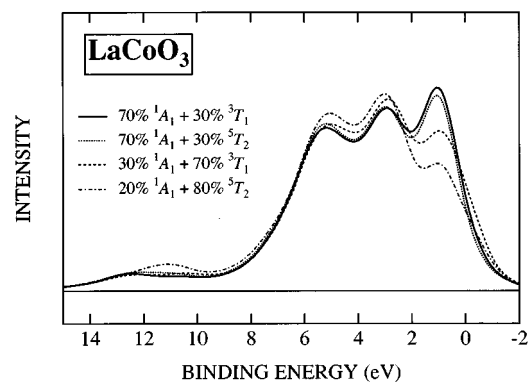


FIG. 8. Simulations of the temperature-dependent XPS spectra of  $\text{LaCoO}_3$  for the two types ( ${}^1A_1 - {}^3T_1$  and  ${}^1A_1 - {}^5T_2$ ) of the mixed initial states. 70%  ${}^1A_1 + 30\%$   ${}^3T_1$  and 70%  ${}^1A_1 + 30\%$   ${}^5T_2$  correspond to  $\sim 80$  K and 30%  ${}^1A_1 + 70\%$   ${}^3T_1$  and 20%  ${}^1A_1 + 80\%$   ${}^5T_2$  correspond to  $\sim 300$  K.

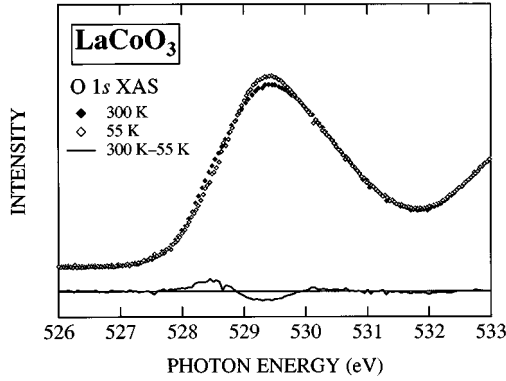


FIG. 9. O 1s XAS spectra of  $\text{LaCoO}_3$  at 55 and 300 K near the threshold. The two spectra have been normalized to the integrated intensity from 526.5 to 533.0 eV. The difference between the high- and low-temperature spectra is also shown.

below room temperature,<sup>40</sup> consistent with the weak temperature dependence of the O 1s XAS spectra.

We have also performed cluster-model calculations for the O 1s XAS spectra of  $\text{LaCoO}_3$  assuming the  $^1A_1$ ,  $^3T_1$ , and  $^5T_2$  initial states, as shown in Fig. 10(a).<sup>41</sup> As in the calculated XPS spectra, the  $^1A_1$  and the  $^3T_1$  spectra are

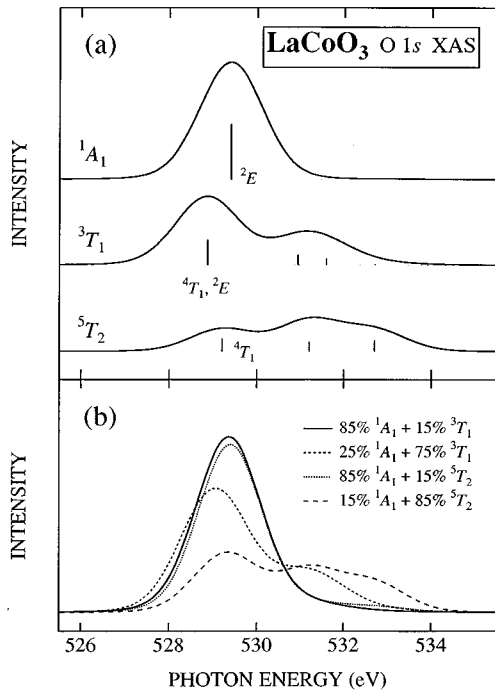


FIG. 10. (a) Full-multiplet cluster-model calculations of the O 1s XAS spectra of  $\text{LaCoO}_3$  assuming the  $^1A_1$ ,  $^3T_1$ , and  $^5T_2$  initial states. The spectra have been shifted so that the  $^2E$  final state is located at 529.4 eV. (b) Simulations of the temperature-dependent O 1s XAS spectra of  $\text{LaCoO}_3$  for the two types ( $^1A_1$ - $^3T_1$  and  $^1A_1$ - $^5T_2$ ) of mixed initial states: 85%  $^1A_1$ +15%  $^3T_1$  and 85%  $^1A_1$ +15%  $^5T_2$  correspond to  $\sim 55$  K and 25%  $^1A_1$ +75%  $^3T_1$  and 15%  $^1A_1$ +85%  $^5T_2$  correspond to  $\sim 300$  K. The ratio has been approximately fixed to reproduce the measured magnitude of the magnetic susceptibility at each temperature (see Fig. 3).

relatively similar to each other, while the  $^5T_2$  spectrum gives different results from the others. Simulations of the temperature-dependent O 1s XAS spectra assuming the two types ( $^1A_1$ - $^3T_1$  and  $^1A_1$ - $^5T_2$ ) of mixed initial states are shown in Fig. 10(b). In both simulations, the  $^2E$  final state peak reduces its intensity from  $\sim 55$  to  $\sim 300$  K and the  $^1A_1$ - $^5T_2$  mixed spectrum shows larger decrease than the  $^1A_1$ - $^3T_1$  mixed spectrum. The experimental spectrum also reduces its peak height (Fig. 9), but the change is quite small. Both simulations show that the intensity on the higher photon energy side of the  $^2E$  final peak increases with temperature, which has not been observed in the experiment. Besides, neither simulation can well explain the growing small shoulder in the experiment at 528.4 eV. The effect of the O 1s core-hole potential may have to be included to quantitatively analyze the O 1s XAS spectra.

### C. Comparison with band-structure calculation

Recently, Hamada, Sawada, and Terakura<sup>13</sup> have performed band-structure calculations for  $\text{LaMO}_3$  ( $M=\text{Ti-Cu}$ ) in the local-spin-density approximation (LSDA) using the full-potential linearized augmented-plane-wave (FLAPW) method. For  $\text{LaCoO}_3$ , they have obtained a nonmagnetic semimetallic ground state. In order to compare their results with our photoemission spectra, we have shifted the conduction bands upwards, taken only the DOS of the occupied bands,<sup>42</sup> and fixed the top of the valence band at 0.4 eV below  $E_F$  to obtain best agreement with the XPS spectrum as shown in Fig. 11.<sup>38,43</sup> It is noted that the activation energy obtained from the resistivity is 0.1–0.25 eV (Refs. 10, 12, and 44) and hence the location of the top of the valence band, 0.4 eV, is too deep. A similar comparison has recently been made by Sarma *et al.*<sup>45</sup>

We have measured high-resolution UPS spectra of  $\text{LaCoO}_3$  at several temperatures. Below 100 K, unfortunately, we could not take reasonable spectra due to charging of the sample. In Fig. 12, one can observe four structures A, B, C, and D as in Fig. 5. A small bump around 9 eV could be interpreted as due to a satellite structure and/or surface degradation. There is very little change in the whole valence band between 100 and 200 K (not shown), except for a slight (a few meV) shift of the whole spectrum towards higher binding energy at 100 K.

In Fig. 12, we compare the UPS spectra of  $\text{LaCoO}_3$  taken at 100 K with the band-structure calculation.<sup>13,46</sup> Here we have used only the (occupied) O  $p$  partial DOS because the Co 3d-to-O 2p relative cross section is only  $\sim 8\%$  around this photon energy.<sup>35</sup> Following the activation energy of the electrical conductivity, which is at most 0.25 eV, we have fixed the top of the valence band in the DOS to 0.25 eV below  $E_F$ . Although the four structures in the calculated DOS can be easily assigned as structures A, B, C, and D, the observed spectral line shape is much broader than the calculated DOS. Especially, the first peak in the band-structure calculation located at  $\sim 0.6$  eV is very sharp while the experimental spectrum shows only a broad peak at  $\sim 1.0$  eV. A possible origin for the discrepancy is a polaronic effect,<sup>47,48</sup> but further studies are necessary to clarify this point.

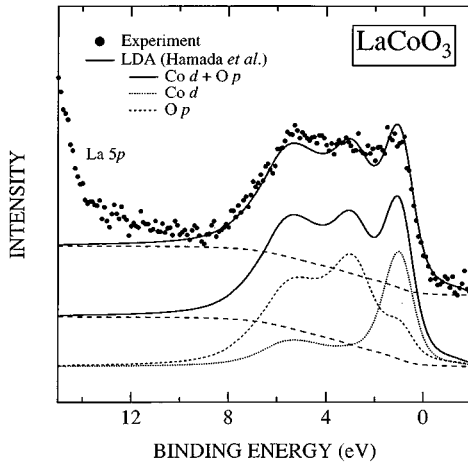


FIG. 11. Valence-band XPS spectrum of  $\text{LaCoO}_3$  compared with the LDA band-structure calculation by Hamada, Sawada, and Terakura (Ref. 13). Simulated valence-band spectra (solid lines) are compared with the experimental spectrum (dots). The Co  $3d$  partial DOS and the O  $2p$  partial DOS are also shown.

#### IV. DISCUSSION

Within the simple ionic model, the  ${}^1A_1$ - ${}^3T_1$  and  ${}^1A_1$ - ${}^3T_1$ - ${}^5T_2$  models can account for the behavior of the magnetic susceptibility of  $\text{LaCoO}_3$  up to around  $\sim 300$  and  $\sim 1000$  K, respectively. On the other hand, the  ${}^1A_1$ - ${}^5T_2$  model needs antiferromagnetic interaction between the  ${}^5T_2$  Co ions in order to explain the small absolute value of the magnetic susceptibility<sup>12,25</sup> whereas the inelastic neutron scattering study has revealed the presence of weak ferromagnetic correlation at  $T \geq 100$  K.<sup>1</sup> The calculated valence-band spectrum assuming the  ${}^1A_1$ - ${}^3T_1$  initial state shows good agreement with the XPS spectrum at  $\sim 80$  K and qualitatively explains the small change in the valence-band spectrum with temperature.<sup>2</sup> As for the O  $1s$  XAS spectra, the  ${}^1A_1$ - ${}^3T_1$  model explains the temperature dependence of the experimental data only qualitatively. We consider that the discrepancy comes from the fact that our calculations do not include the effect of the O  $1s$  core-hole potential in the final state of the x-ray absorption process. A main shortcoming of the  ${}^1A_1$ - ${}^3T_1$  model is that the  ${}^3T_1$  state is located higher than the  ${}^5T_2$  state according to the CI cluster-model calculation with reasonable parameter values, possibly due to the limitation of the single-site cluster model: the LDA+ $U$  calculation has found the IS state to be the first excited state.<sup>15</sup> According to the Hartree-Fock calculations,<sup>16</sup> too, the total energy of the IS state can be considerably lowered by an ordering of the  $e_g$  orbitals. Further, the Hartree-Fock calculations predict that the system becomes a ferromagnetic metal in the orbital-ordered IS state, consistent with the weak ferromagnetic correlation observed by the neutron scattering study.<sup>1</sup> Therefore, we consider that the magnetic transition of  $\text{LaCoO}_3$  at  $\sim 90$  K is not the  ${}^1A_1$ -to- ${}^5T_2$  transition but the  ${}^1A_1$ -to- ${}^3T_1$  transition. The optical studies have shown that the charge gap is  $\sim 0.1$  eV,<sup>12,49</sup> which is larger than the spin gap  $\sim 0.03$  eV,<sup>12</sup> suggesting that the lowest excited state is an excitonic bound state of an electron-hole pair with local

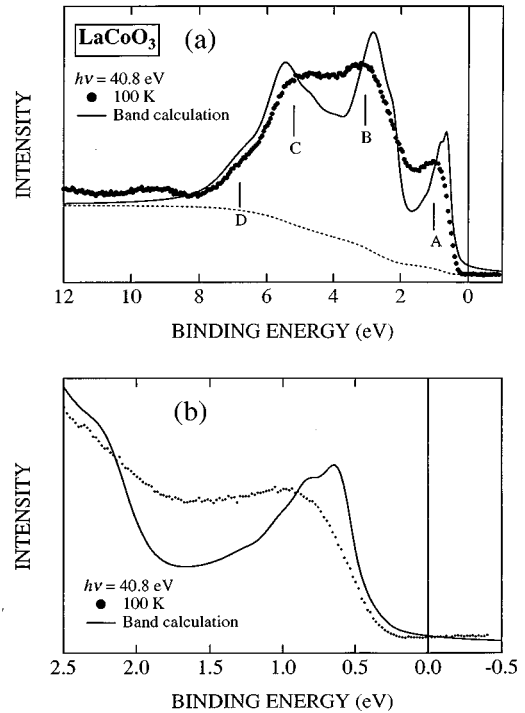


FIG. 12. Comparison between the high-resolution UPS spectra of  $\text{LaCoO}_3$  at 100 K and the LDA band-structure calculation by Hamada, Sawada, and Terakura (Ref. 13). (a) Wide range. (b) Near  $E_F$ .

magnetic moment. This localized magnetic excitation may be spread over several sites due to the strong hybridization between the Co  $3d$  and O  $2p$  orbitals and stabilized by inter-cluster effects such as (short-range) orbital ordering.

The alternative approach to the electronic structure of  $\text{LaCoO}_3$  is the itinerant band picture, starting from the calculated LDA band structure. Except for the satellite structure, the band calculation also shows good agreement with the XPS spectrum. Consequently, if one introduces correlation effects into the band structure as a self-energy correction, one may have another description of  $\text{LaCoO}_3$ .<sup>16</sup> Along this line, the magnetic susceptibility may be calculated by spin-fluctuation theory as in the case of FeSi.<sup>50</sup> In fact, both  $\text{LaCoO}_3$  and FeSi can be considered as strongly correlated semiconductors from the fact that their magnetic and electrical properties at finite temperatures deviate from those of conventional semiconductors. While the spin gap is much smaller than the charge gap in  $\text{LaCoO}_3$ , FeSi (Ref. 51) has similar magnitudes of the spin and charge gaps, indicating that there are no bound electron-hole pairs in the excited states of FeSi and hence that interaction between quasiparticles is weaker in FeSi than in  $\text{LaCoO}_3$ . Thus the band-structure calculation is certainly a better starting point for FeSi than for  $\text{LaCoO}_3$ . For FeSi, the observed band edge is shifted *towards*  $E_F$  compared to the band DOS, which indicates a band *narrowing* and enables us to analyze the spectra using a dynamical, local self-energy correction.<sup>51</sup> On the other hand, the band edge is shifted *away from*  $E_F$  compared to the LDA result in  $\text{LaCoO}_3$  (Fig. 12), indicating a band *widening*.

## V. CONCLUSIONS

We have studied the electronic structure of  $\text{LaCoO}_3$  by photoemission spectroscopy and x-ray absorption spectroscopy and analyzed them in terms of the local cluster CI model. The Co  $2p$  core-level and the valence-band photoemission spectra display satellite structures. The  $^1A_1$  ground state of  $\text{LaCoO}_3$  is found to consist of  $\sim 30\%$   $d^6$ ,  $\sim 50\%$   $d^7\bar{L}$ , and  $\sim 20\%$   $d^8\bar{L}^2$  states, indicating a strongly hybridized ground state.  $\text{LaCoO}_3$  is a charge-transfer-type insulator, but the band gap has considerable  $p$ - $p$  character due to the strong hybridization. From the cluster-model analysis of the spectra as well as the analysis of the magnetic susceptibility, the magnetic transition in  $\text{LaCoO}_3$  at  $\sim 90$  K seems most likely due to the  $^1A_1$ -to- $^3T_1$  transition although agreement between theory and experiment is not yet satisfactory for the spectral line shapes.

## ACKNOWLEDGMENTS

We would like to thank Y. Tezuka and S. Shin of SRL and Y. Azuma of PF for technical support. We are grateful to Y. Murakami for support in the SQUID measurement and K. Kobayashi, A. Ino, C. Fukushima, and K. Morikawa for assistance in the measurements and the analyses. We would like to thank N. Hamada for providing their numerical data of the band-structure calculations. We would also like to thank T. Katsufuji, Y. Okimoto, and D. D. Sarma for valuable discussions. Part of this work has been done under the approval of the Photon Factory Program Advisory Committee (Proposal No. 94G361). Part of the calculations in this work have been performed using a VAX/VMS system at the Meson Science Laboratory, Faculty of Science, University of Tokyo. The present work is supported by the Japan Society for the Promotion of Science for Japanese Junior Scientists, a Grant-in-Aid for Scientific Research from the Ministry of Education, Science and Culture and the New Energy and Industrial Technology Development Organization (NEDO).

\*Present address: Department of Physics, University of Colorado, Boulder, Colorado 80309-0390, U.S.A.

<sup>1</sup>K. Asai, P. Gehring, H. Chou, and G. Shirane, *Phys. Rev. B* **40**, 10 982 (1989); K. Asai, O. Yokokura, N. Nishimori, H. Chou, J. M. Tranquada, G. Shirane, S. Higuchi, Y. Okajima, and K. Kohn, *ibid.* **50**, 3025 (1994).

<sup>2</sup>M. Abbate, J. C. Fuggle, A. Fujimori, L. H. Tjeng, C. T. Chen, R. Potze, G. A. Sawatzky, H. Eisaki, and S. Uchida, *Phys. Rev. B* **47**, 16 124 (1993).

<sup>3</sup>J. B. Goodenough and P. M. Raccach, *J. Appl. Phys. Suppl.* **36**, 1031 (1965); P. M. Raccach and J. B. Goodenough, *Phys. Rev.* **155**, 932 (1967).

<sup>4</sup>G. H. Jonker and J. H. van Santen, *Physica* **19**, 120 (1953).

<sup>5</sup>R. R. Heikes, R. C. Miller, and R. Mazelsky, *Physica* **30**, 1600 (1964).

<sup>6</sup>W. C. Koehler and E. O. Wollan, *J. Phys. Chem. Solids* **2**, 100 (1957); N. Menyuk, K. Dwight, and P. M. Raccach, *ibid.* **28**, 549 (1967).

<sup>7</sup>C. S. Naiman, R. Gilmore, B. DiBartolo, A. Linz, and R. Santoro, *J. Appl. Phys.* **36**, 1044 (1965); G. H. Jonker, *ibid.* **37**, 1424 (1966).

<sup>8</sup>G. Thornton, B. C. Tofield, and A. W. Hewat, *J. Solid State Chem.* **61**, 301 (1986).

<sup>9</sup>M. Itoh, I. Natori, S. Kubota, and K. Motoya, *J. Phys. Soc. Jpn.* **63**, 1486 (1994).

<sup>10</sup>V. G. Bhide, D. S. Rajoria, G. Rama Rao, and C. N. R. Rao, *Phys. Rev. B* **6**, 1021 (1972).

<sup>11</sup>G. Thornton, B. C. Tofield, and D. E. Williams, *Solid State Commun.* **44**, 1213 (1982).

<sup>12</sup>S. Yamaguchi, Y. Okimoto, H. Taniguchi, and Y. Tokura, *Phys. Rev. B* **53**, 2926 (1996).

<sup>13</sup>N. Hamada, H. Sawada, and K. Terakura, in *Spectroscopy of Mott Insulators and Correlated Metals*, edited by A. Fujimori and Y. Tokura (Springer-Verlag, Berlin, 1995) p. 95.

<sup>14</sup>M. Abbate, R. Potze, G. A. Sawatzky, and A. Fujimori, *Phys. Rev. B* **49**, 7210 (1994).

<sup>15</sup>M. A. Korotin, S. Yu. Ezhov, I. V. Solovyev, V. I. Anisimov, D. I. Khomskii, and G. A. Sawatzky, *Phys. Rev. B* **54**, 5309 (1996).

<sup>16</sup>T. Mizokawa and A. Fujimori, *Phys. Rev. B* **54**, 5368 (1996).

<sup>17</sup>G. Thornton, A. F. Orchard, and C. N. R. Rao, *J. Phys. C* **9**, 1991 (1976).

<sup>18</sup>B. W. Veal and D. J. Lam, *J. Appl. Phys.* **49**, 1461 (1978); D. J. Lam, B. W. Veal, and D. E. Ellis, *Phys. Rev. B* **22**, 5730 (1980).

<sup>19</sup>L. Richter, S. D. Bader, and M. B. Brodsky, *Phys. Rev. B* **22**, 3059 (1980).

<sup>20</sup>J. P. Kemp, D. J. Beal, and P. A. Cox, *J. Solid State Chem.* **86**, 50 (1990); G. Thornton, I. W. Owen, and G. P. Diakun, *J. Phys. Condens. Matter* **3**, 417 (1991).

<sup>21</sup>A. Chainani, M. Mathew, and D. D. Sarma, *Phys. Rev. B* **46**, 9976 (1992).

<sup>22</sup>S. Masuda, M. Aoki, Y. Harada, H. Hirohashi, Y. Watanabe, Y. Sakisaka, and H. Kato, *Phys. Rev. Lett.* **71**, 4214 (1993).

<sup>23</sup>S. R. Barman and D. D. Sarma, *Phys. Rev. B* **49**, 13 979 (1994).

<sup>24</sup>D. B. Chestnut, *J. Chem. Phys.* **40**, 405 (1964); R. A. Bari and J. Sivardiére, *Phys. Rev. B* **5**, 4466 (1972); R. Zimmermann and E. König, *J. Phys. Chem. Solids* **7**, 779 (1977).

<sup>25</sup>M. Itoh, M. Sugahara, I. Natori, and K. Motoya, *J. Phys. Soc. Jpn.* **64**, 3967 (1995).

<sup>26</sup>T. Saitoh, A. E. Bocquet, T. Mizokawa, and A. Fujimori, *Phys. Rev. B* **52**, 7934 (1995).

<sup>27</sup>T. Saitoh, A. E. Bocquet, T. Mizokawa, H. Namatame, A. Fujimori, M. Abbate, Y. Takeda, and M. Takano, *Phys. Rev. B* **51**, 13 942 (1995).

<sup>28</sup>A. E. Bocquet, T. Mizokawa, T. Saitoh, H. Namatame, and A. Fujimori, *Phys. Rev. B* **46**, 3771 (1992).

<sup>29</sup>A. Fujimori and F. Minami, *Phys. Rev. B* **30**, 957 (1984).

<sup>30</sup>The Lorentzian FWHM is taken to be  $1.8+0.15\Delta E$  (eV), where  $\Delta E$  is the energy separation from the lowest binding energy peak, and the Gaussian FWHM to be  $\sim 2.8$  eV.

<sup>31</sup>L. F. Mattheiss, *Phys. Rev. B* **5**, 290 (1972); W. A. Harrison, *Electronic Structure and the Properties of Solids* (Dover, New York, 1989).

<sup>32</sup>T. Mizokawa, H. Namatame, A. Fujimori, K. Akeyama, H. Kon-doh, and N. Kosugi, *Phys. Rev. Lett.* **67**, 1638 (1991).

<sup>33</sup>Chainani, Mathew, and Sarma (Ref. 21) have analyzed the Co  $2p$  core-level photoemission spectrum of  $\text{LaCoO}_3$  using the cluster model, and obtained somewhat different parameter values  $\Delta=4.0$  eV,  $U=3.4$  eV, and  $(pd\sigma)=-2.2$  eV. These parameters, however, give a ground state with 39%  $d^6$ , 45%  $d^7\bar{L}$ , and 15%  $d^8\bar{L}^2$  similar to the present results, indicating a very strongly mixed ground state. We consider that the differ-

- ence between their parameter values and ours comes mainly from the following reasons: They have not considered the difference between the different Coulomb integrals, assumed an additional crystal field  $10Dq = 1.0$  eV, and fixed the energy difference between the oxygen  $t_{2g}$  and  $e_g$  states at 1.5 eV while no  $10Dq$  and no splitting of the oxygen states are included in our SSD scheme calculations. They fixed  $U$  at the value that they obtained from comparison of the Co  $L_3M_{45}M_{45}$  Auger spectrum with the self-convolution of the valence-band XPS spectrum. This  $U$  was smaller than ours, and needed a large ( $pd\sigma$ ) in order to obtain a good fit with experiment.
- <sup>34</sup>T. Mizokawa and A. Fujimori, *Phys. Rev. B* **48**, 14 150 (1993).
- <sup>35</sup>J. J. Yeh and I. Lindau, *At. Data Nucl. Data Tables* **32**, 1 (1985).
- <sup>36</sup>The Lorentzian FWHM is taken to be  $0.46 + 0.1\Delta E$  (eV) and the Gaussian FWHM to be  $\sim 1.5$  eV.
- <sup>37</sup>The He I spectrum has been broadened by a Lorentzian function with FWHM of 0.37 eV and a Gaussian function with FWHM of 0.70 eV in order to simulate the XPS spectrum.
- <sup>38</sup>The binding-energy ( $E$ )-dependent Lorentzian FWHM is assumed to be  $0.36 + 0.1(E - E_F)$  (eV), where 0.36 eV is the lifetime width of the Mg  $K\alpha$  line, and the Gaussian FWHM to be 0.9 eV.
- <sup>39</sup>We have included the empirical multiplication factor of  $\sim 3$  for the O  $2p$  states. This empirical factor has been successfully used in previous studies on transition-metal oxides [H. Eisaki, S. Uchida, T. Mizokawa, H. Namatame, A. Fujimori, J. van Elp, P. Kuiper, G. A. Sawatzky, S. Hosoya, and H. Katayama-Yoshida, *Phys. Rev. B* **45**, 12 513 (1992); Ref. 27; Ref. 29].
- <sup>40</sup>Y. Okimoto, T. Katsufuji, S. Yamaguchi, and Y. Tokura (private communication).
- <sup>41</sup>The Lorentzian FWHM is taken as  $0.01 + 0.01\Delta E$  (eV), and the Gaussian FWHM as  $\sim 1.7$  eV.
- <sup>42</sup>We have used the numerical data of the DOS by courtesy of Dr. N. Hamada. He kindly divided their data into the occupied and unoccupied bands.
- <sup>43</sup>The O  $2p$ -to-Co  $3d$  intensity ratio, which gives the best fit to the experiment had to be taken 2.9 times as large as the CI cluster-model calculation. One reason for the large multiplication factor for the O  $2p$  intensity is that the O  $2p$  partial DOS was underestimated due to the much smaller oxygen muffin-tin radius (0.85 Å) than the Co muffin-tin radius (1.06 Å) (Ref. 42).
- <sup>44</sup>S. Yamaguchi, Y. Okimoto, and Y. Tokura, *Phys. Rev. B* **54**, R11 022 (1996).
- <sup>45</sup>D. D. Sarma, N. Shanthi, S. R. Barman, N. Hamada, H. Sawada, and K. Terakura, *Phys. Rev. Lett.* **75**, 1126 (1995).
- <sup>46</sup>The Lorentzian FWHM is assumed to be  $8.5 + 0.08(E - E_F)$  (meV), where 8.5 meV is the lifetime width of the He II line, and the Gaussian FWHM to be 0.9 eV.
- <sup>47</sup>H. Namatame, A. Fujimori, H. Takagi, S. Uchida, F. M. F. de Groot, and J. C. Fuggle, *Phys. Rev. B* **48**, 16 917 (1993).
- <sup>48</sup>A. Fujimori, A. E. Bocquet, K. Morikawa, K. Kobayashi, T. Saitoh, Y. Tokura, I. Hase, and M. Onoda, *J. Phys. Chem. Solids* **57**, 1379 (1996).
- <sup>49</sup>T. Arima, Y. Tokura, and J. B. Torrance, *Phys. Rev. B* **48**, 17 006 (1993).
- <sup>50</sup>Y. Takahashi and T. Moriya, *J. Phys. Soc. Jpn.* **46**, 1452 (1979); Y. Takahashi, M. Tano, and T. Moriya, *J. Magn. Magn. Mater.* **31-34**, 329 (1983).
- <sup>51</sup>T. Saitoh, A. Sekiyama, T. Mizokawa, A. Fujimori, K. Ito, H. Nakamura, and M. Shiga, *Solid State Commun.* **95**, 307 (1995).